Frey, F.A., Coffin, M.F., Wallace, P.J., and Quilty, P.G. (Eds.)
Proceedings of the Ocean Drilling Program, Scientific Results Volume 183

12. Identifying Magnetic Carriers from Rock Magnetic Characterization of Leg 183 Basement Cores[1]

Xixi Zhao,[2] Maria Antretter,[3] Peter Solheid,[4] and Hiroo Inokuchi[5]

ABSTRACT

In this manuscript, we present rock magnetic results of samples recovered during Leg 183. The Leg 183 cores were recovered from six drill sites and display variable rock magnetic properties. The differences in the rock magnetic properties are a function of mineralogy and alteration. Cretaceous subaerial basalt samples with titanomagnetite exhibit a strong Verwey transition in the vicinity of 110 K and have frequency-dependent susceptibility curves that resemble those of synthetic (titano) magnetites. These results are in good agreement with the thermomagnetic characteristics where titanomagnetites with Curie temperatures of ~580ºC were identified. The hysteresis ratios suggest that the bulk magnetic grain size is in the psuedo-single-domain boundary. These subaerial basalts experienced high-temperature oxidation and maintained reliable paleomagnetic records. In contrast, the 34-Ma submarine pillow basalts do not show the Verwey transition during the low-temperature experiments. Thermomagnetic analysis shows that the remanent magnetization in this group is mainly carried by a thermally unstable mineral titanomaghemite. The frequency-dependent relationships are opposite of those from the first group and show little sign of titanomagnetite characteristics. Rocks from the third group are oxidized titanomagnetites and have multiple magnetic phases. They have irreversible thermaomagnetic curves and hysteresis ratios clustering toward the multidomain region (with higher H_{cr}/H_c ratios).

The combined investigation suggests that variations in magnetic properties correlate with changes in lithology, which results in differences in the abundance and size of magnetic minerals. The rock mag-

[1]Zhao, X., Antretter, M., Solheid, P., and Inokuchi, H., 2002. Identifying magnetic carriers from rock magnetic characterization of Leg 183 basement cores. *In* Frey, F.A., Coffin, M.F., Wallace, P.J., and Quilty, P.G. (Eds.), *Proc. ODP, Sci. Results,* 183, 1–28 [Online]. Available from World Wide Web: <http://www-odp.tamu.edu/publications/183_SR/VOLUME/CHAPTERS/005.PDF>. [Cited YYYY-MM-DD]
[2]Center for the Study of Imaging and Dynamics of the Earth, Institute of Geophysics and Planetary Geophysics, University of California, Santa Cruz CA 95064, USA. **xhao@es.ucs.edu**
[3]Institut fur Allgemeine und Angewandte Geophysik, Ludwig-Maximilians-Universitat Munchen, Theresienstrasse 41, 80333 Munchen, Germany.
[4]Institute for Rock Magnetism, 291 Shepherd Laboratories, University of Minnesota, Minneapolis MN 55455, USA.
[5]School of Humanity, Environment Policy, and Technology
Himeji Institute of Technology
Shinzaikehonmachi 1-1-12
Himeji, Hyogo 670-0092, Japan.

Initial receipt: 24 June 2002
Acceptance: 14 May 2002
Web publication: 4 December 2002
Ms 183SR-005

netic data on Leg 183 samples clearly indicate that titanomagnetite is the dominant mineral and the primary remanence carrier in subaerial basalt. The generally good magnetic stability and other properties exhibited by titanomagnetite-bearing rocks support the inference that the ChRM isolated from the Cretaceous sites were acquired during the Cretaceous Normal Superchron. The stable inclinations identified from these samples are therefore useful for future tectonic studies.

INTRODUCTION

Ocean Drilling Program (ODP) Leg 183 is the first thematic leg to investigate the history of the Kerguelen Plateau/Broken Ridge, an example of unique Cretaceous emplacement of a large igneous province (LIP) in the southern Indian Ocean (Fig. **F1**). Understanding the origin and evolutionary history of the Kerguelen Plateau is of particular importance because it has been suggested to link to the onset of the Kerguelen-Heard mantle plume (e.g., Storey et al., 1989). The structurally complex Kerguelen Plateau has been divided into southern, central, and northern domains. Preliminary interpretations of the results of Leg 183 suggest that the age of the Southern Kerguelen Plateau, only hundreds of kilometers from Antarctica, formed 119 m.y. ago. To the north, the Central Kerguelen Plateau and the once-contiguous Broken Ridge and Elan Bank formed between 94 and 110 m.y. ago. In contrast, the Northern Kerguelen Plateau is much younger, having formed <35 m.y. ago (Coffin, Frey, Wallace, et al., 2000; Frey et al., 2000; Pringle and Duncan, 2000). These results indicate that several intense episodes of volcanism formed this large plateau over a long period of time, in contrast with the case for the Ontong Java Plateau in the Pacific, where the plateau appears to have formed mainly in a single massive volcanic event at ~122 Ma (Parkinson et al., 2001).

During Leg 183, the changes in magnetic and physical properties of basement rocks have been investigated by whole-core measurements of magnetic susceptibility, natural remanent magnetization (NRM), and compressional wave velocity. In general, we observed that for subaerial basalts the brecciated flow tops have higher susceptibilities and stronger NRM intensities than the massive interiors. Submarine lava flows display the opposite behavior; altered pillow rims have lower susceptibilities and NRM intensities than the massive pillow interiors. On the other hand, changes in compressional wave velocity show the same general trend for both subaerial and submarine basaltic rocks: the least-altered massive interior samples have velocities greater than the flow tops, which are highly altered (Coffin, Frey, Wallace, et al., 2000). Although these trends are consistent with observations reported in previous studies (e.g., Audunsson et al., 1992; Planke et al., 1999), further shore-based rock magnetic studies are needed to correctly identify the magnetic minerals, to explore the relationship between magnetic properties and lithology and alteration, and to evaluate the fidelity of the natural magnetic memory in the basalt rocks from the Kerguelen Plateau/Broken Ridge.

The purpose of this paper is to present the results of such a rock magnetic investigation carried out on basement cores recovered from Leg 183 sites. Additional work on the sediments of these sites is presented in **Antretter et al.** (this volume). We will first describe the rock magnetic results, focusing on the cores that provided the most readily inter-

F1. Map of eastern Indian Ocean, p. 15.

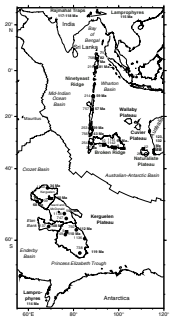

pretable data. We will then discuss and interpret the data in conjunction with lithology, alteration, and oxidation.

SITE AND BASEMENT LITHOLOGY

During Leg 183, we penetrated igneous basement at five sites on the Kerguelen Plateau and two sites on Broken Ridge. The site locations (Fig. F1) and drilling results are documented in detail in the site chapters of the Leg 183 *Initial Reports* volume and other appropriate papers (see Coffin, Frey, Wallace, et al., 2000; Frey et al., 2000). A simplified summary of the drill sites is given in Table T1. The lithology and paleoenvironment of the sites will be briefly mentioned here.

T1. Summary of Leg 183 drill sites, p. 24.

Drilling at Site 1136 in the southern Kerguelen Plateau recovered three inflated pahoehoe basalt flows similar to continental flood basalts (Table T1). Generally, these flows show a vertical zonation with a bubbly vesicular top, a fresh massive interior, and a fine-grained and vesicle-rich base typical of subaerial flows. At Site 1137 on the Elan Bank, drilling recovered 151.7 m of a basement sequence, which contains seven basaltic lava flows and three interbedded volcaniclastic sediment units. The interiors of the seven lava flows from Site 1137 are relatively unaltered and similar to those from Site 1136, but the volcanic sediments are highly altered and weathered. The inflated pahoehoe characteristics of the seven lava flows and the fluvial environment of the volcaniclastic sedimentary rocks strongly indicate subaerial eruption of the basalts. At Site 1138 on the central Kerguelen Plateau, we recognized 22 units within the 144 m of igneous basement drilled. These are tholeiitic basalt flows whose compositions define a systematic downhole trend to Fe- and Ti-rich basalt (Coffin, Frey, Wallace, et al., 2000). Alteration ranges from high to complete in the brecciated zones with flow tops partly and completely altered to clay minerals. Site 1138 was above sea level during its construction. Site 1139 was drilled on Skiff Bank of the northern Kerguelen Plateau. Basement rocks recovered include variably welded trachytic and rhyolitic volcanic and volcaniclastic rocks and lava flows. All basement units are altered and fractured at Site 1139. Site 1139 was also subaerial during its final stages of formation. At Site 1140, which lies on the northernmost Kerguelen Plateau, drilling recovered 49.1 m of basement rocks, which includes five submarine basaltic flows and a layer of dolomitized nannofossil chalk, in contrast with all other basement sites drilled at the Kerguelen Plateau. Alteration of Site 1140 lavas strongly resembles that of young mid-ocean-ridge pillows (Coffin, Frey, Wallace, et al., 2000). It is worth noting that Site 1140 is situated at 2394 m, whereas seafloor depths at all other basement sites are much shallower (between 1000 and 2000 m) (Table T1).

Sites 1141 and 1142 are situated near the crest of Broken Ridge (Fig. F1). Initial interpretation of cores suggests that most of the basaltic lavas at Sites 1141 and 1142 were erupted subaerially, but there is also a hint that Site 1142 possibly erupted in submarine environment (Coffin, Frey, Wallace, et al., 2000). The tops of most volcanic units at Site 1141 have been highly to completely altered to clay. Red flow tops and green to gray flow interiors suggest decreasing oxidation with depth. The lithology and alteration intensity at Site 1142 are heterogeneous. Some units are massive and slightly altered, whereas other volcanic units are variably brecciated by both tectonic and volcanic processes and are highly to completely altered. The difference between igneous basement

sections at these two sites may be a result of penetration of different stratigraphic levels or considerable unanticipated lateral variability in volcanism (Coffin, Frey, Wallace, et al., 2000).

METHODS

One of the major experimental requirements in paleomagnetic research is to isolate the characteristic remanent magnetization (ChRM) by selective removal of secondary magnetization. To investigate the nature of the remanent magnetization of the basement rocks at Kerguelen Plateau, discrete samples were alternating-field (AF) or thermally demagnetized during shipboard study. A total of 169 discrete paleomagnetic samples were used for shore-based rock magnetic studies. The rock magnetic data presented in this paper are from measurements performed at the paleomagnetism laboratories at University of California at Santa Cruz (UCSC), University of Munich in Germany, and the Institute for Rock Magnetism at the University of Minnesota. For rock magnetic characterization, samples were subjected to a wide range of magnetic measurements. These included (1) Curie temperature determinations using both low and high applied fields (0.05 mT and 1 T, respectively); (2) hysteresis loop parameter measurements: saturation magnetization (J_s), saturation remanence (J_r), coercivity (H_c), and remanent coercivity (H_{cr}) as a function of temperature (10–400 K); (3) saturation isothermal remanent magnetization (SIRM) as a function of temperature (10–300 K); (4) alternating-current (AC) susceptibility measurements as a function of field amplitude and field frequency; and (5) Mössbauer spectroscopy. A brief description of each experiment is given below.

The Curie temperature is the temperature below which a magnetic mineral is magnetically ordered. For an example, when a magnetite sample is heated to a temperature of ~580°C (the Curie point for magnetite), it loses all its remanent magnetization. This loss in spontaneous magnetization is due to thermal agitations overcoming the exchange energy. Because the Curie temperature is a sensitive indicator of composition, it is useful in understanding the magnetic mineralogy. In this study, Curie temperatures were determined by measurement of low-field magnetic susceptibility or induced moment vs. temperature (using both the Kappabridge susceptometer at UCSC and the Princeton Micro-Mag vibrating sample magnetometer at the University of Minnesota). To avoid oxidation that could lead to chemical alteration, we conducted thermomagnetic analyses in an inert helium or argon atmosphere on 105 samples representative of Leg 183 cores. We used a graphic method (Grommé et al., 1969) that uses the intersection of two tangents to the thermomagnetic curve that bounds the Curie temperature to determine the Curie temperature. This method is most straightforward to perform by hand, although it tends to underestimate Curie temperatures with the two other methods presented by Moskowitz (1981) and Tauxe (1998).

To further understand the magnetic properties and estimate the domain structure of magnetic minerals, room-temperature hysteresis loops were measured on representative samples. Hysteresis loop parameters are useful in characterizing the intrinsic magnetic behavior of rocks. Thus, they are helpful in studying the origin of remanence. In this study, hysteresis loops and the associated parameters J_r, J_s, H_c, and H_{cr} were obtained using Princeton Measurements Corporation alternat-

ing gradient magnetometers (AGFM) capable of resolving magnetic moments as small as 5×10^{-8} emu (Flanders, 1988). Saturation magnetization (J_s) is the largest magnetization a sample can have. The coercivity (H_c) is a measure of magnetic stability. The two ratios, J_r/J_s and H_{cr}/H_c, are commonly used as indicators of domain states and, indirectly, grain size. For magnetite, high values of J_r/J_s (>0.5) indicate small (<0.1 µm or so) single-domain (SD) grains, and low values (<0.1) are characteristic of large (>15–20 µm) multidomain grains (MD). The intermediate regions are usually referred to as pseudo single-domain (PSD). H_{cr}/H_c is a much less reliable parameter, but conventionally SD grains have a value close to 1.1, and MD grains should have values >3–4 (Day et al., 1977; Dunlop, 2002). Hysteresis parameters for 106 representative samples were determined at the University of California, Santa Cruz, the University of Munich in Germany, and the University of Minnesota. For a selected group of samples, we also examined the change of hysteresis loops during warming from 10 to 400 K (at intervals of 10 K).

Low-temperature measurements were made on 31 representative samples to help characterize the magnetic minerals and understand their rock magnetic properties. These measurements were designed to determine the Néel temperature and other critical temperatures of a magnetic substance. The measurements were made from 10 K to room temperature (300 K) on 100- to 300-mg subsamples in a quantum design magnetic property measurement system (MPMS) at the University of Minnesota. Samples were given an SIRM in a steady magnetic field of 2.5 T at 300 K and cooled in a zero field to 20 K; the remanence was measured at 5-K intervals. The sample was then given an SIRM in a field of 2.5 T before being warmed to 300 K in zero field while measuring the remanence value every 5 K in sweep measurement fashion. Unlike high-temperature measurements, there is no risk of oxidizing the sample because it is at low temperature and is not heated.

To investigate the field- and frequency-dependent susceptibility of the Leg 183 cores, AC susceptibility measurements were made on a few selected samples with a LakeShore Model 7130 AC susceptometer and the MPMS at the University of Minnesota. The temperature dependence of the in-phase (m') and quadrature (m'') mass susceptibility between 15 and 300 K was measured at five frequencies (40, 140, 400, 1000, and 4000 Hz), with AC field amplitudes between 100 and 1000 A/m.

Two samples were selected for Mössbauer effect investigation to provide another means of identifying magnetic carriers in basalts from the Kerguelen Plateau and Broken Ridge. Measurements were taken at room temperature using ^{57}Co in a rhodium source and a constant acceleration spectrometer. A crushed sample (~0.5 g in powder form) was packed into a polythene sample holder with a cross-sectional area of ~1 cm^2.

RESULTS

Paleomagnetism

During our shipboard paleomagnetic studies for Leg 183, we characterized the stable components of NRM through thermal and AF demagnetization. Details are illustrated and described in the site chapters of the Leg 183 *Initial Reports* volume (Coffin, Frey, Wallace, et al. 2000). Here, we only highlight the most relevant points in terms of demagnetization behavior, paleolatitude, and magnetic polarity.

A stable component of magnetization in the basement rocks from Sites 1136, 1137, 1138, 1139, and 1140 was revealed. In most samples, this stable component of magnetization was straightforward upon AF or thermal treatments. A generally minor secondary component, probably a viscous overprint from the recent field, was present in some samples but was easily removed at peak fields of 20 mT or at a low temperature of ~150°C. The median destructive fields ranged mostly in the 30- to 50-mT interval, suggesting the existence of small pseudosingle grains as remanence carriers (Dunlop and Özdemir, 1997). Most samples have unblocking temperatures of ~580°C, suggesting titanium-poor titanomagnetite is responsible for the remanent magnetization. In some samples, we observed two magnetic phases during stepwise thermal demagnetization and susceptibility measurements. A high-temperature phase is characterized by an unblocking temperature of ~580°C, and a low-temperature phase is characterized by an unblocking temperature of ~300°C. In a few samples, the stable component was not unblocked until 620°C. Magnetic susceptibilities for these samples increased at 400°–500°C and decreased at 500°–620°C, indicating changes from (titano)maghemite to (titano)magnetite and then to (titano)maghematite, respectively.

The magnetically cleaned mean inclinations at Sites 1136 and 1137 correspond to paleolatitudes that are ~4°–10° farther north than present-day site latitudes. Assuming the inclination represents the primary remanence at the time when these rocks were formed, the paleolatitude results would suggest that the southern Kerguelen Plateau and Elan Bank have moved southward since Cretaceous time. This southward movement seems to be consistent with previous paleomagnetic results from the southern Kerguelen Plateau, which show a difference of 13°–16° between present day latitude and paleolatitude of basement rocks (Inokuchi and Heider, 1992).

The ChRM for Sites 1136 (119 Ma), 1137 (108 Ma), 1138 (100 Ma), 1141 (95 Ma), and 1142 (95 Ma) are all normal, which may indicate the magnetization was acquired during the Cretaceous Normal Superchron (121–83 Ma) and is also consistent with the ages of the rocks. However, there is no independent proof of this timing, as no meaningful fold tests are available on the basement rocks. Thus, the normal magnetization could be an overprint resulting in the acquisition of secondary magnetization, which is now accepted as a widespread phenomenon (e.g., Van der Voo, 1993). Interestingly, preliminary shipboard paleomagnetic studies on six samples from Site 1139 (68 Ma) showed reversed polarity magnetization. There is also a magnetic reversal zone at the boundary between basement rock Units 1 and 2 at Site 1140 (34 Ma) (Shipboard Scientific Party, 2000b). The main issues that are important to consider are the timing of the reversal zones in the basalt (i.e., whether it is the same as the formation of the basalts) and the ability of basalts to carry the remanent magnetization (i.e., whether it is stable over geologically significant time intervals). Additional rock magnetic data are needed to constrain the observed reversal polarity zone.

Rock Magnetic Properties

Curie Temperature Determination of Samples

Curie temperature determinations of samples from Sites 1136–1142 are presented in Table T2. Strong field thermomagnetic curves were obtained to determine the magnetic phases in the samples. According to

T2. Summary of Curie temperature determination, p. 25.

Curie temperatures (Table T2), three different groups can be recognized from the Leg 183 samples. Group l (Fig. F2A) is characterized by a single ferromagnetic phase with Curie temperatures between 480° and 580°C, compatible with that of Ti-poor titanomagnetites. The cooling and heating curves are reasonably reversible. Most subaerial flows from Sites 1136, 1137, 1138, 1139, 1141, and 1142 belong to this group (Table T2). Group 2 has lower Curie temperatures (165°–359°C) (see Table T2) that are typical of titanium-rich titanomagnetite (such as TM60) or low-temperature oxidized titanomaghemites. Group 2 curves (Fig. F2B) were mainly observed for pillow basalts from Site 1140. Other rock samples that can be included in this group are from the lower parts of Sites 1136 and 1138, which exhibit similar low Curie temperatures. Samples 183-1136A-19R-1, 122–124 cm; 183-1138A-88R-1, 53–55 cm; and 183-1138A-89R-3, 40–42 cm, are exceptions (Table T2). Samples belonging to Group 3 have multiple magnetic phases and come mainly from Site 1139. For the purpose of showing the entire suite of measurements from one representative sample, we choose to show Sample 183-1138A-85R-2, 89–91 cm, which displays the same behavior. The irreversible thermomagnetic curve of this sample displays one magnetic phase with Curie temperature of ~380°C on heating (Fig. F2C). The second highest Curie temperature phase is observed at ~540°C. The large difference between heating and cooling of the sample suggests that a low-temperature oxidized titanomagnetite is the main magnetic mineral.

Comparison of the two Curie temperatures (obtained by low-field continuous susceptibility and high-field magnetic moment vs. temperature runs) reveals that, in general, Curie temperature by susceptibility as a function of temperature is less than those determined by high-field magnetic moment runs (Table T2). An extreme discrepancy in Curie temperatures is presented by Sample 183-1140A-37R-4, 16–18 (Table T2). The strong-field Curie temperature is found to be 540°C, which is consistent with titanomagnetite 05, but the susceptibility data are flat after 230°C. It is not clear whether this is due to nonhomogeneous subsamples used in the two instruments. Thermomagnetic curves for the two crystal vitric tuff samples (Table T2) from Site 1137 show behavior that cannot be interpreted in a simple manner. The magnetic mineralogy for these two samples is complex, and the results are not readily explained at present.

F2. Thermomagnetic curves for Leg 183 basalts, p. 16.

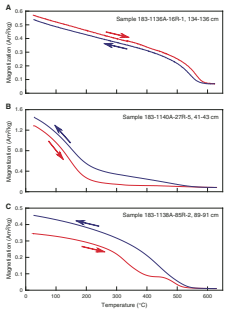

Hysteresis Loop Parameters

The samples analyzed in this study indicate that subaerial basalt samples from Sites 1136, 1137, 1138, and 1141 show the predominance of the PSD size, probably indicating a mixture of MD and SD grains (Fig. F3). We note that if some superparamagnetic grains are also present, the measured coercive force and saturation magnetization may be somewhat lower and larger, respectively. The magnetic grain sizes of the pillow basalt samples from Site 1140 fall near the boundary between SD and PSD. In contrast, samples from Sites 1139 and 1142 distribute toward the boundary between PSD and MD, with a few samples even falling in the MD size (Fig. F3; Table T3). All the samples from Site 1139 also showed constricted hysteresis loops (or "wasp-waisted" loops), indicating multiple magnetic phases. The corresponding hysteresis ratios (Fig. F3; Table T3) appear to suggest the secondary magnetite formation reported by various colleagues (e.g., Channel and McCabe, 1994). Examples of a room-temperature hysteresis loop from the Kerguelen Pla-

F3. Hysteresis ratios, p. 17.

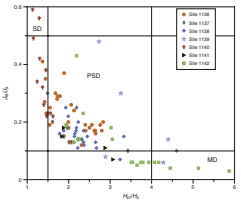

T3. Summary of hysteresis properties, p. 27.

teau for representative basalt samples that exhibit SD, MD, and PSD behavior are shown in Figure F4.

For a selected group of samples, we also examined the change of hysteresis loops as a function of temperature (10–400 K) to detect changes in the domain state at low or high temperature. Figure F5 shows selected hysteresis loops for two representative samples. The nonsaturating linear part in the subaerial basalt sample (Sample 183-1136A-15R-3, 109-111 cm) indicates a paramagnetic component (Fig. F5A). After that, loop parameters for this sample show little temperature variant. On the other hand, the fine-grained pillow basalt sample (Sample 183-1140A-27R-5, 41–43 cm) displayed a different domain structure (Fig. F5B). In this sample, coercivity and saturation remanence measured at each temperature from the hysteresis loop exhibit similar dependences on temperature for a TM60 sample from the Mogo Hill breccia (M. Jackson, pers. comm., 2000), with a rapid drop between 10 and 80 K. It is interesting to note that coercivity increases from 10 to 50 K then decreases at higher temperatures (Fig. F5B). Hysteresis loops for Sample 183-1139A-71R-4, 8–9 cm, maintained superparamagnetic loops throughout the entire temperature interval.

Low-Temperature Properties

As shown in Figure F6, the low-temperature curves of SIRM both in zero field warming and cooling display a variety of features. These include an unblocking temperature in the vicinity of 40–50 K, which is probably caused by superparamagnetic magnetite particles (Moskowitz et al., 1993) and a decrease in remanence in the 100–120 K range, which is most likely caused by the Verwey transition (Verwey et al., 1947). Figure F6A shows cooling and warming curves for Sample 183-1136A-16R-1, 134–136 cm, which has PSD grain size. Remanence is lost at ~110–120 K as the sample cools and warms through the Verwey transition. On the other hand, no obvious Verwey transition is observed for the pillow basalt sample (Sample 183-1140A-27R-5, 41–43 cm) during cooling to 19 K. Upon warming from 19 K, however, a distinctive bend in remanence is present near 100 K. With continued warming, the decay of remanence is almost linear all the way to room temperature (Fig. F6B).

Figure F6C shows a third behavior. Sample 183-1138A-85R-2, 81–91 cm, has smaller grain size as indicated by hysteresis measurement. A rapid decrease in remanence between 10 and 40 K is observed (Fig. F6C). A similar phenomenon was observed in the study of oxidized synthetic magnetite by Özdemir et al. (1993) and was attributed to the presence of an ultra fine-grained superparamagnetic phase with a very low unblocking temperature. No pronounced remanence transition is observed, although the sample displays a more rapid decrease of remanence between 50 and 120 K. In comparison with the classic Verwey transition, the remanence transition for this sample is perhaps blurred over a broad temperature interval and is shifted toward lower temperatures. The low-temperature magnetometry is one of the major lines of evidence for the division of these three different groups.

Low-Temperature AC Susceptibility Measurements

Figures F7 and F8 show examples of the temperature dependence of magnetic susceptibility between 15 and 300 K for two Leg 183 core samples. The frequency-dependent susceptibility curves for the subaerial

F4. Room-temperature hysteresis loop, p. 18.

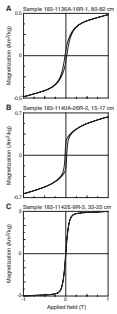

F5. Hysteresis behavior of selected samples, p. 19.

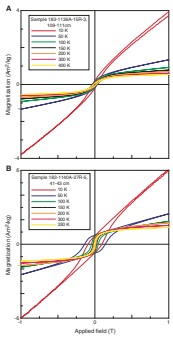

F6. Low-temperature heating curves of saturation remanence, p. 20.

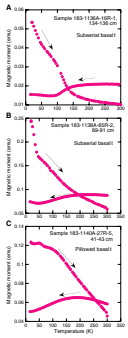

F7. Temperature dependence of mass susceptibility, Sample 183-1141A-24R-2, 6-8 cm, p. 21.

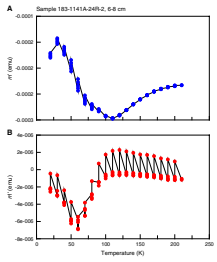

basalt sample (Sample 183-1141A-24R-2, 6–8 cm) from Site 1141 (Broken Ridge) are generally similar to those of synthetic titanomagnetite 28 and 41 (TM28 and TM41) (Jackson et al., 1998), with some frequency dependence from 25 to 100 K. An abrupt decrease of in-phase susceptibility (m') is observed at ~40 K. Susceptibility then increases through the Verwey transition to 120 K. There is an abrupt frequency dependence increase between 55 and 95 K (see the lower part of the diagram in Fig. F7), a feature that is not yet understood. The frequency dependence of quadrature (m'') susceptibility observed from 100 to 200 K may indicate the presence of superparamagnetic grains. Interestingly, the fine-grained pillow basalt sample (Sample 183-1140A-37R-4, 16-18 cm) from Site 1140 (northern Kerguelen Plateau) shows very different frequency-dependent susceptibility curves (Fig. F8). There is no detectable frequency dependence of susceptibility until after 250 K, probably because the susceptibility is a superposition of paramagnetic and ferrimagnetic susceptibilities from different Fe-bearing phases.

F8. Temperature dependence of mass susceptibility, Sample 183-1140A-37R-4, 16-18 cm, p. 22.

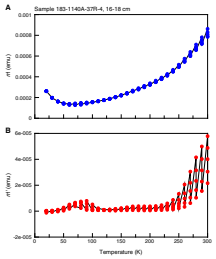

Mössbauer Effect Spectrometry

The Mössbauer spectra obtained for the two samples that reflect the differences in the Leg 183 lithologies are shown in Figure F9. The spectrum of a subaerial basalt sample (Sample 183-1136A-16R-2, 140–142 cm) from Site 1136 (the Kerguelen Plateau) is shown in Figure F9A. At room temperature, the spectrum is dominated by three magnetically ordered components that have been tentatively identified as magnetite, maghemite, and hematite, respectively. The magnetite spectrum contains two components, one corresponding to the A site (Fe^{3+}) and the other to the B site. Figure F9B shows the spectrum of a subaerial basalt sample from the Broken Ridge area (Sample 183-1141A-24R-2, 6–8 cm) with fitted curves. The values of the fitting parameters for this spectrum suggest two components that can be identified as maghemite and magnetite, respectively.

F9. Mössbauer spectra, p. 23.

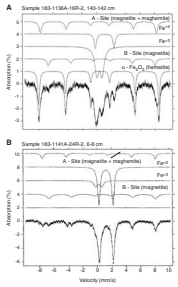

DISCUSSION

The results described above have revealed important information about the origin of remanence and magnetic minerals present in the Leg 183 cores. The Leg 183 cores recovered from the six drilling sites displayed variable rock magnetic properties. Three general types of behavior were found in the rock magnetic measurements. One group has a single phase of Ti-poor titanomagnetite. The majority of subaerial basaltic samples from Sites 1136, 1137, 1138, 1141, and 1142 belong to this group. Results for various massive subaerial basalt samples (Table T2) show Curie temperatures between 480° and 605°C, compatible with those of Ti-poor titanomagnetites. The thermomagnetic curves of these samples exhibit very little difference between heating and cooling of the samples. Samples with titanomagnetite also exhibit a strong Verwey transition in the vicinity of 110 K and frequency-dependent susceptibility curves that resemble those of synthetic Ti-poor titanomagnetites. These results are in good agreement with the hysteresis ratios suggesting that the bulk magnetic grain size is in the PSD boundary (e.g., with lower H_{cr}/H_c values). Subaerial basalts have been thoroughly studied (e.g., Lindsley, 1962; Grommé et al., 1969; Ade-Hall et al., 1971; Tucker and O'Reilly, 1980). They have high Curie temperatures (500°–580°C) and rarely have two Curie points (Dunlop and Özdemir, 1997). They

undergo deuteric high-temperature oxidation, which is responsible for the high Curie temperature. It is this high-temperature oxidation, especially when carried to completion with the production of fine-grained hematite, that makes subaerial basalts excellent recorders of the geomagnetic field (Dunlop and Özdemir, 1997). In this regard, a subaerial sample (Sample 183-1136A-16R-2, 140–142 cm) from Site 1136 may have experienced the high-temperature oxidation, as the Mössbauer spectrum of this sample shows sign of presence of hematite. Therefore, the subaerial basalts from this group are most likely good paleomagnetic recorders that can preserve original and stable magnetic remanences.

The second group is characterized by a Curie temperature of 200°–400ºC and is mainly represented by pillow basalt samples from Site 1140. Samples in this group apparently went through low-temperature oxidation, which is another form of alteration for titanomagnetite (Dunlop and Özdemir, 1997). Thermomagnetic analysis using the low-field susceptibility method shows that the remanent magnetization in this group is carried by a thermally unstable mineral that breaks down at ~400ºC. Thermomagnetic analysis using the high-temperature vibrating sample magnetometer shows evidence for unoxidized titanium-rich titanomagnetite (TM60) (Fig. F2B). The low-temperature curves for this sample and the rest of the samples of the group do not show Verwey transition. The frequency-dependent relationships are distinctly different from those in the first group and show little or no sign of pure titanomagnetite characteristics. The magnetic grain sizes of the pillow basalt samples fall toward the boundary between SD and PSD with several samples fall in the SD size (Fig. F3). The rock magnetically inferred fine grain size indicates a rapid cooling environment for the pillow lavas of Site 1140. Altogether, these rock magnetic data seem to be sensitive indicators of low-temperature oxidation and support the contention that titanium-rich titanomagnetite is responsible for the magnetic signatures displayed in the pillow basalts.

The third group has more than one Curie temperature, which suggests the presence of multiple magnetic phases. Four of the six samples from Site 1139 (Table T2) belong to this group. Although the hysteresis ratios for rocks in this group still fall in the PSD region, the cluster is centered toward the MD region (with higher H_{cr}/H_c ratios). Low-temperature curves do not clearly show the Verwey transition (Fig. F6C). The thermomagnetic signature indicates the inversion of titanomaghemite to a strongly magnetized magnetite, as showing by the irreversible cooling curve (Fig. F2C). Although chemical remanent magnetization resulting from oxidization of titanomagnetite and inversion of titanomaghemite has been shown to parallel the original thermoremance (Johnson and Merrill, 1974; Hall, 1977; Özdemir and Dunlop, 1985; Dunlop and Özdemir, 1997), it is difficult to assess whether these rocks retain stable remanent magnetization from the data collected in this study.

Variations of Curie temperatures also suggest that a stratigraphically distinct change in magnetic minerals exists in Leg 183 drill sites. It is significant to note that the variations come from relatively deeper sections of the basement that coincide with changes in lithology and alteration. For example, rocks in the lower part of Site 1136 basement exhibit lower Curie temperatures (Sections 183-1136A-18R-2 through 19R-2) (see Table T2). Preliminary shipboard observations also show that vesicle distribution in these cores increases significantly, from 1% in the overlying sections to 10%–15% (Shipboard Scientific Party,

2000a). The vesicles and veins are filled with dark olive-green clays, which not only suggests that alteration is most likely the product of both weathering and low-temperature fluid-rock reaction but also emphasizes the importance of distinctions between primary and secondary causes of magnetic property variation.

Although not every problem in paleomagnetism has a rock magnetic solution, there is clearly a strong interest in constraining remanent magnetization by detailed rock magnetic studies (e.g., Banerjee, 1992). Measurement of rock magnetic parameters has been demonstrated to be useful for studying various rock-forming and rock-altering geological processes. The results described in this study have revealed important information about the origin of remanence and the magnetic minerals present in the Leg 183 cores. The rock magnetic data from Leg 183 samples clearly indicate that titanomagntite is the dominant mineral and the primary remanence carrier. The generally good magnetic stability and other properties exhibited by these rocks support the inference that the ChRM isolated from the Cretaceous sites were acquired during the Cretaceous Normal Superchron. The stable inclinations identified from these samples are therefore useful for future tectonic studies.

The rapidly cooled pillow basalt samples from Site 1140 (34 Ma) are fresh to slightly altered and have a more uniform magnetic grain size distribution. From the high-field magnetic moment curves and Curie points, it may be inferred that Ti-rich titanomagnetites are present in these submarine basalts and they are expected to give accurate results. Basalts recovered at Site 1142 were questioned as pillowed basalts in the shipboard petrological description (see Table **T2**). Results of our rock magnetic investigation on a limited set of these rocks, however, would suggest they were most likely erupted in a subaerial environment, which is similar to their counterpart at Site 1141.

Most of samples from Site 1139 showed the third group behavior, which raises the question of whether the reversed signal observed in six Site 1139 cores is due to field or self reversals. We do not believe these samples have a self-reversed thermal remanent magnetization because the thermal magnetic curves for the normal and reversed magnetized samples are indistinguishable. However, we noticed that Site 1139 lies on the Skiff Bank, which has been proposed as the current site of the Kerguelen hotspot. Although hundreds of meters of sediment on parts of the elevated feature argue against the Skiff Bank originating entirely as a result of recent volcanism, the shipboard petrologic observation for these altered volcanic rocks and trachyte basalt favor the hypothesis that the remanence may be a recent overprint during alteration. Magnetic grain-size measurements in this study, as determined from hysteresis ratios, show that the magnetic minerals of Site 1139 cores are of PSD–MD size and have undergone low-temperature oxidation. This information, together with other observations and a lack of evidence to the contrary, would suggest that substantial alteration has subsequently taken place and may have reset the original magnetization. Thus, we favor the speculation that the reversed magnetization in the six samples from Site 1139 involves resetting of the direction of remanence by alteration. Additional work is still needed to constrain the magnetic interpretation.

CONCLUSIONS

This study has demonstrated the potential value of paleomagnetic, rock magnetic, and geological investigations in providing the essential link between remanence magnetization, rock magnetic property variations, and magnetic mineralogy. Based on rock magnetic results obtained during our postcruise study of Leg 183 cores, we can draw the following conclusions:

1. The majority of subaerial basalt samples from Sites 1136 (119 Ma), 1137 (108 Ma), 1138 (100 Ma), 1141 (95 Ma), and 1142 (95 Ma) underwent deuteric high-temperature oxidation, which is responsible for the high Curie temperature. These subaerial basalts are probably good paleomagnetic recorders that can preserve original and stable magnetic remanences.
2. The rock magnetically inferred fine grain size indicates a rapid cooling environment for the pillow lavas of Site 1140 (34 Ma). The generally good magnetic stability exhibited by the titanomagnetite-bearing rocks suggests that the stable inclinations identified from these submarine samples are useful for future tectonic studies.
3. Although rocks at Site 1142 were listed as possible pillow basalt, rock magnetic data suggest they are probably same as their counterpart at Site 1141, erupted in a subaerial environment. Their normal magnetic polarity supports the inference that the ChRM isolated from the 95-Ma rocks were acquired during the Cretaceous Normal Superchron (121–83 Ma).
4. Basalt flows at Site 1139 underwent low-temperature oxidation. Substantial alteration at this site has subsequently taken place and may have reset the original magnetization.

ACKNOWLEDGMENTS

This research used samples and/or data provided by the Ocean Drilling Program (ODP). ODP is sponsored by the U.S. National Science Foundation (NSF) and participating countries under management of Joint Oceanographic Institution (JOI), Inc. Financial support for various parts of this research was provided by a grant to X. Zhao from the U.S. Science Support Program of the JOI and NSF grants EAR 443549-22178 and 443747-22035. Funding was also provided by the Center for the Study of Imaging and Dynamics of the Earth, Institute of Geophysics and Planetary Physics at the University of California Santa Cruz, contribution number 449. We would like to thank S. Brachfeld, P. Quilty, and an anonymous reviewer for insightful reviews and constructive suggestions on the original manuscript as well as Millard F. Coffin of the volume editorial board for his help with Figure F1. Thanks to Peter and Janna Riisager for helping with different figures. X. Zhao also wishes to express his appreciation to the shipboard scientists, the ODP marine technicians, and the crew of the *JOIDES Resolution* for their help during Leg 183. We also wish to express our appreciation to the shore-based ODP staff for all of their precruise and postcruise efforts.

REFERENCES

Ade-Hall, J.M., Palmer, H.C., and Hubbard, T.P., 1971. The magnetic and opaque petrological response of basalts to regional hydrothermal alteration. *Geophys. J. R. Astron. Soc.,* 24:137–174.

Audunsson, H., Levi, S., and Hodges, F., 1992. Magnetic property zonation in a thick lava flow. *J. Geophys. Res.,* 97:4349–4360.

Banerjee, S.K., 1992. Applied rock magnetism in the 1990's: potential breakthrough in a new user-driven science. *Eos,* 73:142–143.

Channell, J.E.T., and McCabe, C., 1994. Comparison of magnetic hysteresis parameters of unremagnetized and remagnetized limestones. *J. Geophys. Res.,* 99:4613–4623.

Coffin, M.F., Frey, F.A., Wallace, P.J., et al., 2000. *Proc. ODP, Init. Repts.,* 183 [CD-ROM]. Available from: Ocean Drilling Program, Texas A&M University, College Station, TX 77845-9547, USA.

Day, R., Fuller, M., and Schmidt, V.A., 1977. Hysteresis properties of titanomagnetites: grain-size and compositional dependence. *Phys. Earth Planet. Inter.,* 13:260–267.

Dunlop, D.J., 2002. Theory and application of the Day plot (M_{rs}/M_s versus H_{cr}/H_c) 1. Theoretical curves and tests using titanomagnetite data. *J. Geophys. Res.,* 107 (Article), 10.1029/2001JB000486.

Dunlop, D.J., and Özdemir, Ö., 1997. *Rock Magnetism: Fundamentals and Frontiers:* Cambridge (Cambridge Univ. Press).

Flanders, P.J., 1988. An alternating-gradient magnetometer. *J. Appl. Phys.,* 63:3940–3945.

Frey, F.A., Coffin, M.F., Wallace, P.J., Weis, D., Zhao, X., et al., 2000. Origin and evolution of a submarine large igneous province: the Kerguelen Plateau and Broken Ridge, southern Indian Ocean. *Earth Planet. Sci. Lett.,* 176:73–89.

Grommé, C.S., Wright, T.L., and Peck, D.L., 1969. Magnetic properties and oxidation of iron-titanium oxide minerals in Alae and Makaopuhi lava lakes, Hawaii. *J. Geophys. Res.,* 74:5277–5293.

Hall, J.M., 1977. Does TRM occur in oceanic layer 2 basalts? *J. Geomagn. Geoelectr.,* 29:411–419.

Inokuchi, H., and Heider, F., 1992. Paleolatitude of the southern Kerguelen Plateau inferred from the paleomagnetic study of Upper Cretaceous basalts. *In* Wise, S.W., Jr., Schlich, R., et al., *Proc. ODP, Sci. Results,* 120: College Station, TX (Ocean Drilling Program), 89–96.

Jackson, M.J., Moskowitz, B.M., Rosenbaum, J., and Kissel, C., 1998. Field-dependence of AC susceptibility in titanomagnetites. *Earth Planet. Sci. Lett.,* 157:129–139.

Johnson, H. P., and Merrill, R. T., 1974. Low temperature oxidation of a single-domain magnetite. *J. Geophys. Res.,* 79:5533–5534.

Lindsley, D.H., 1962. Investigations in the system $FeO\text{-}Fe_2O_3\text{-}TiO_2$. *Year Book–Carnegie Inst. Washington,* 61:100–106.

Moskowitz, B.M., 1981. Methods for estimating Curie temperatures of titanomaghemites from experimental J_s- T data. *Earth Planet. Sci. Lett.,* 53:84–88.

Moskowitz, B.M., Frankel, R.B., and Bazylinski, D.A., 1993. Rock magnetic criteria for the detection of biogenic magnetite. *Earth Planet. Sci. Lett.,* 120:283–300.

Parkinson, I.J., Schaefer, B.F. and ODP Leg 192 Shipboard Scientific Party, 2001. A lower mantle origin for the world's biggest LIP? A high precision Os isotope isochron from Ontong Java Plateau basalts drilled on ODP Leg 192. *Eos,* 82:1398.

Planke, S., Cerney, B., Bücker, C. J., and Nilsen, O., 1999. Aleration effects on petrophysical properties of subaerial flood basalts: Site 990, Southeast Greenland margin. *In* Larsen, H.C., Duncan, R.A., Allan, J.F., and Brooks, K. (Eds.), *Proc. ODP, Sci. Results,* 163: College Station, TX (Ocean Drilling Program), 17–28.

Özdemir, O., and Dunlop, D.J., 1985. An experimental study of chemical remanent magnetizations of synthetic monodomain titanomaghemites with initial thermoremanent magnetizations. *J. Geophys. Res.,* 90:11513–11523.

Özdemir, Ö., Dunlop, D.J., and Moskowitz, B.M., 1993. The effect of oxydation on the Verwey transition in magnetite. *Geophys. Res. Lett.,* 20:1671–1674.

Pringle, M.S., and Duncan, R.A., 2000. Basement ages from the Southern and Central Kerguelen Plateau: initial products of the Kerguelen large igneous province. *Eos,* 81:424.

Shipboard Scientific Party, 2000a. Site 1136. *In* Coffin, M.F., Frey, F.A., Wallace, P.J., et al., *Proc. ODP, Init. Repts.,* 183, 1–122 [CD-ROM]. Available from: Ocean Drilling Program, Texas A&M University, College Station, TX 77845-9547, U.S.A.

————, 2000b. Site 1140. *In* Coffin, M.F., Frey, F.A., Wallace, P.J., et al., *Proc. ODP, Init. Repts.,* 183, 1–122 [CD-ROM]. Available from: Ocean Drilling Program, Texas A&M University, College Station, TX 77845-9547, U.S.A.

Storey, M., Saunders, A.D., Tarney, J., Gibson, I.L., Norry, M.J., Thirlwall, M.F., Leat, P., Thompson, R.N., and Menzies, M.A., 1989. Contamination of Indian Ocean asthenosphere by the Kerguelen-Heard mantle plume. *Nature,* 338:574–576.

Tauxe, L., 1998. *Paleomagnetic Principles and Practice:* Dordrecht, Netherlands (Kluwer Academic Publishers.

Tucker, P., and O'Reilly, W.O., 1980. The laboratory simulation of deuteric oxidation of titanomagnetites: effect on magnetic properties and stability of thermoremanence. *Phys. Earth Planet. Inter.,* 23:112–133.

Van der Voo, R., 1993. *Paleomagnetism of the Atlantic, Tethys and Iapetus Oceans:* Cambridge (Cambridge Univ. Press).

Verwey, E.J., Haayman, P.W., and Romeijn, F.C., 1947. Physical properties and cation arrangements of oxides with spinal structure. *J. Chem. Phys.,* 15:181–187.

Figure F1. Map of the eastern Indian Ocean showing major physiographic features and proposed Leg 183 sites where igneous basement was recovered from the Ninetyeast Ridge, Broken Ridge, and Kerguelen Plateau by Deep Sea Drilling Project and ODP drilling (circles) and dredging (squares). Rajmahal Traps, lamprophyres, and Bunbury Basalt (BB) are continental volcanics that have been postulated to be related to the Kerguelen plume. Star = a proposed location (Skiff Bank) for the Kerguelen hotspot (Coffin, Frey, Wallace, et al., 2000).

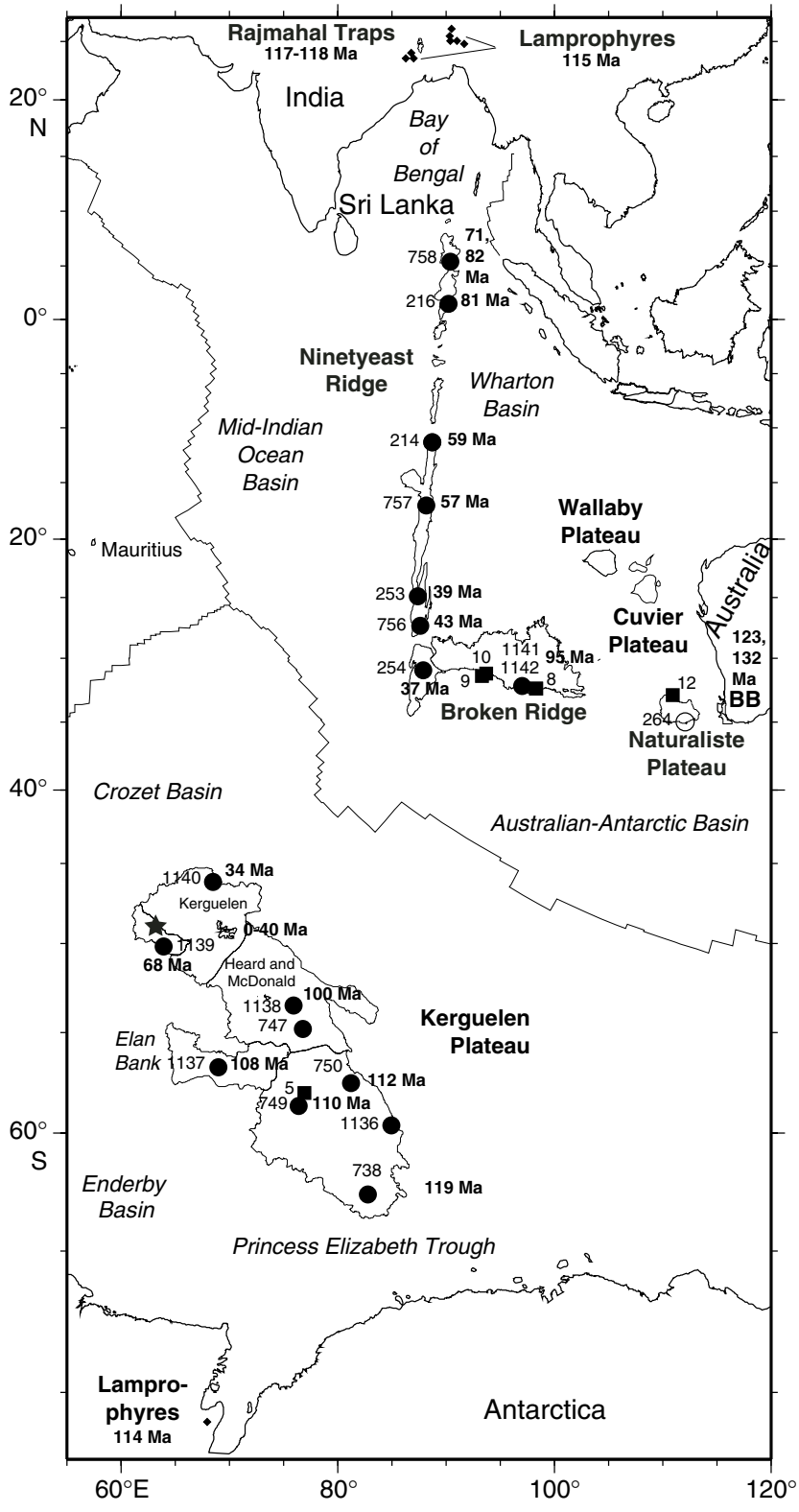

Figure F2. Typical thermomagnetic curves for Leg 183 basalts. (**A**) Subaerial basalt Sample 183-1136A-16R-1, 134–136 cm, (**B**) pillowed basalt Sample 183-1140A-27R-5, 41–43 cm, and (**C**) subaerial basalt Sample 183-1138A-85R-2, 89–91 cm. Red curve = heating, blue curve = cooling.

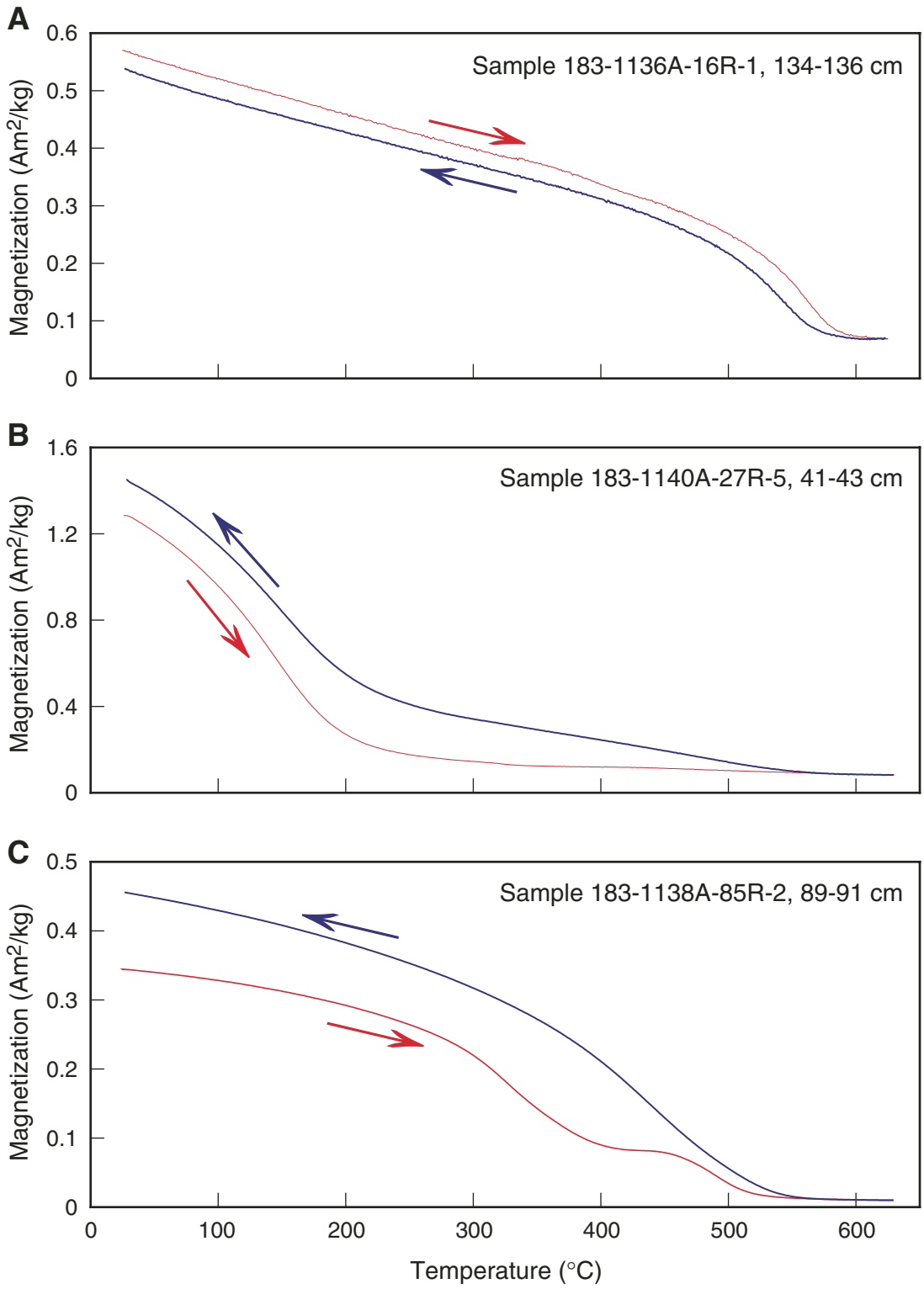

Figure F3. Hysteresis ratios plotted on a Day-type diagram (Day et al., 1977) for basement samples from Leg 183 drill sites. J_s = saturation magnetization, J_r = saturation remanent magnetization, H_c = coercivity, H_{cr} = remanent coercive force. The plot is usually divided into regions: single domain (SD) for $J_s/J_r > 0.5$ and $H_{cr}/H_c < 1.5$, multidomain (MD) for $J_s/J_r < 0.05$ and $H_{cr}/H_c > 4$, and pseudo single-domain (PSD) in between.

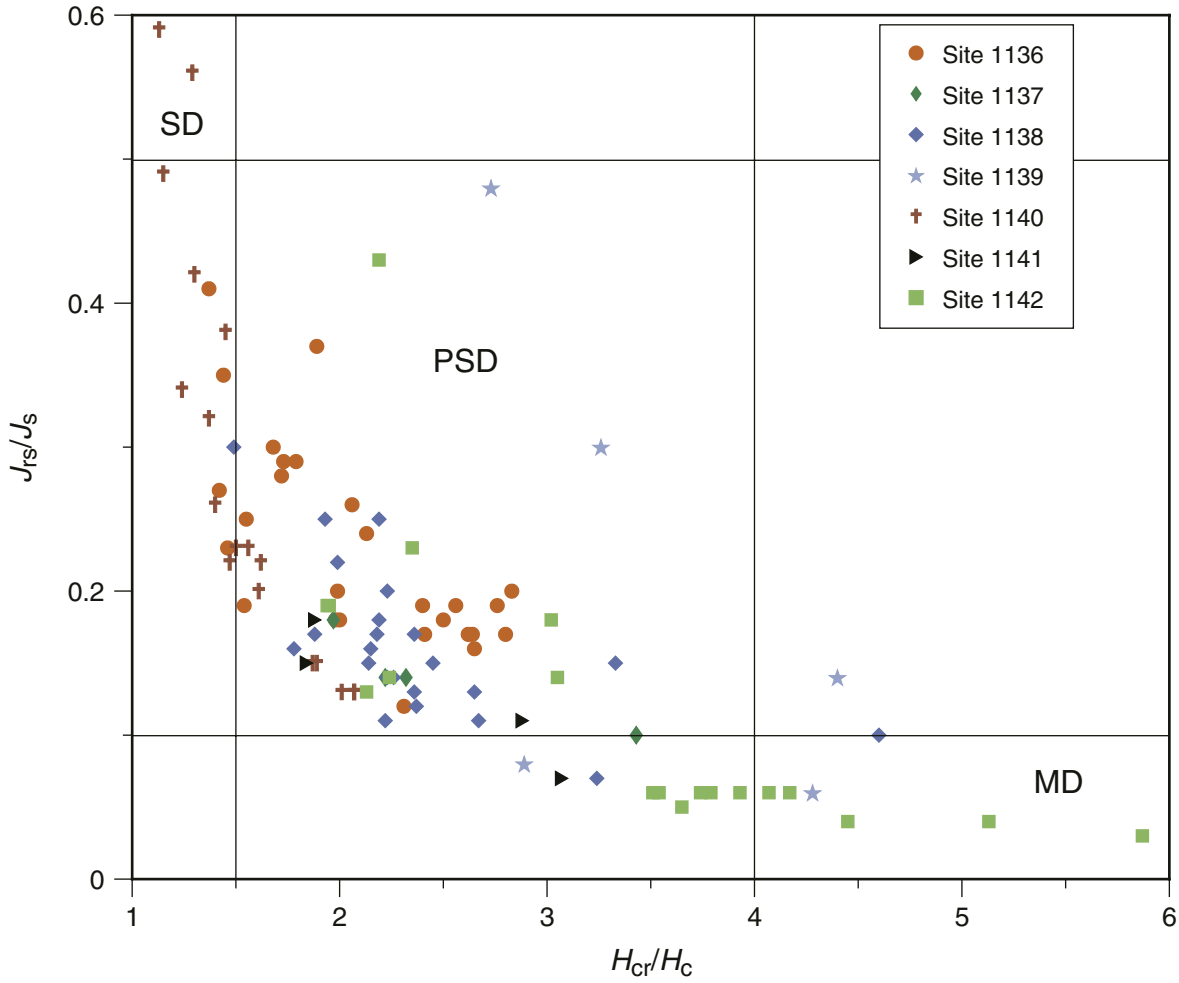

Figure F4. Diagram of room-temperature hysteresis loop for representative basalt samples that exhibit SD, PSD, and MD behavior. (**A**) PSD Sample 183-1136A-16R-1, 80–82 cm, (**B**) SD Sample 183-1140A-26R-2, 15–17 cm, and (**C**) MD Sample 183-1142A-9R-3, 33–35 cm. Horizontal axis is applied field up to 1 T. Vertical axis is mass-specific magnetization (corrected for slope).

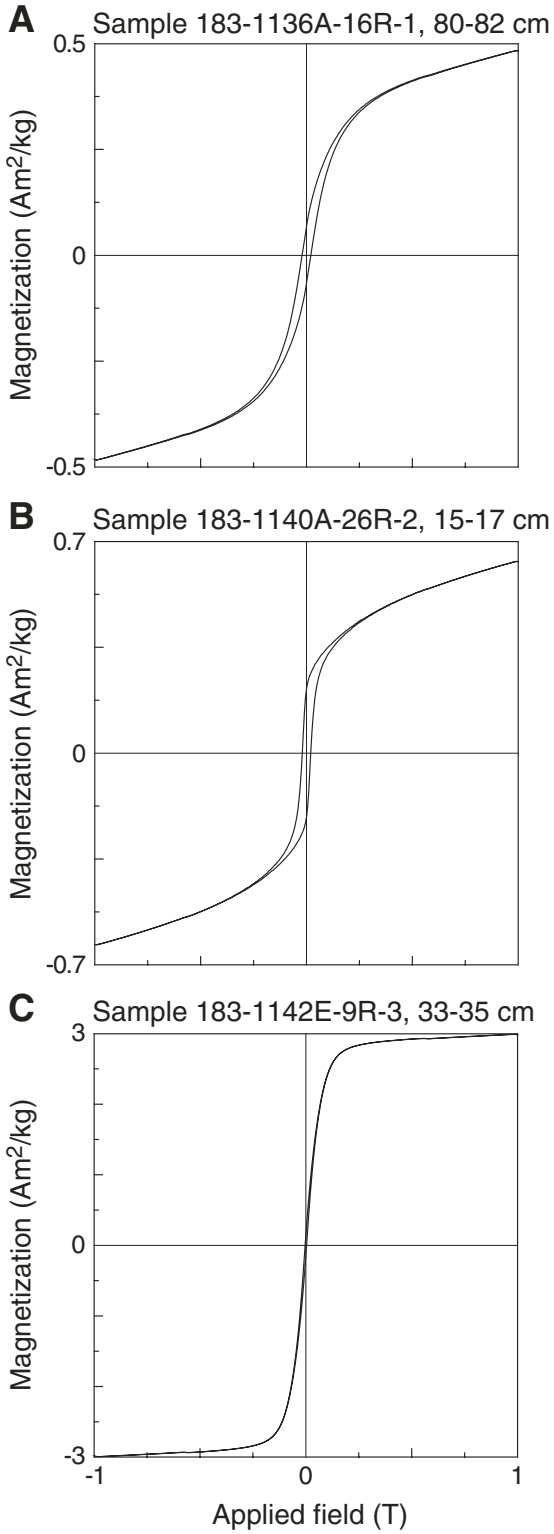

Figure F5. Diagram of hystersis behavior of selected samples during warming from 10 to 400 K. (**A**) Subaerial basalt Sample 183-1136A-15R-3, 109–111 cm, and (**B**) pillowed basalt Sample 183-1140A-27R-5, 41–43 cm. Horizontal axis = applied field up to 1 T, vertical axis = magnetization.

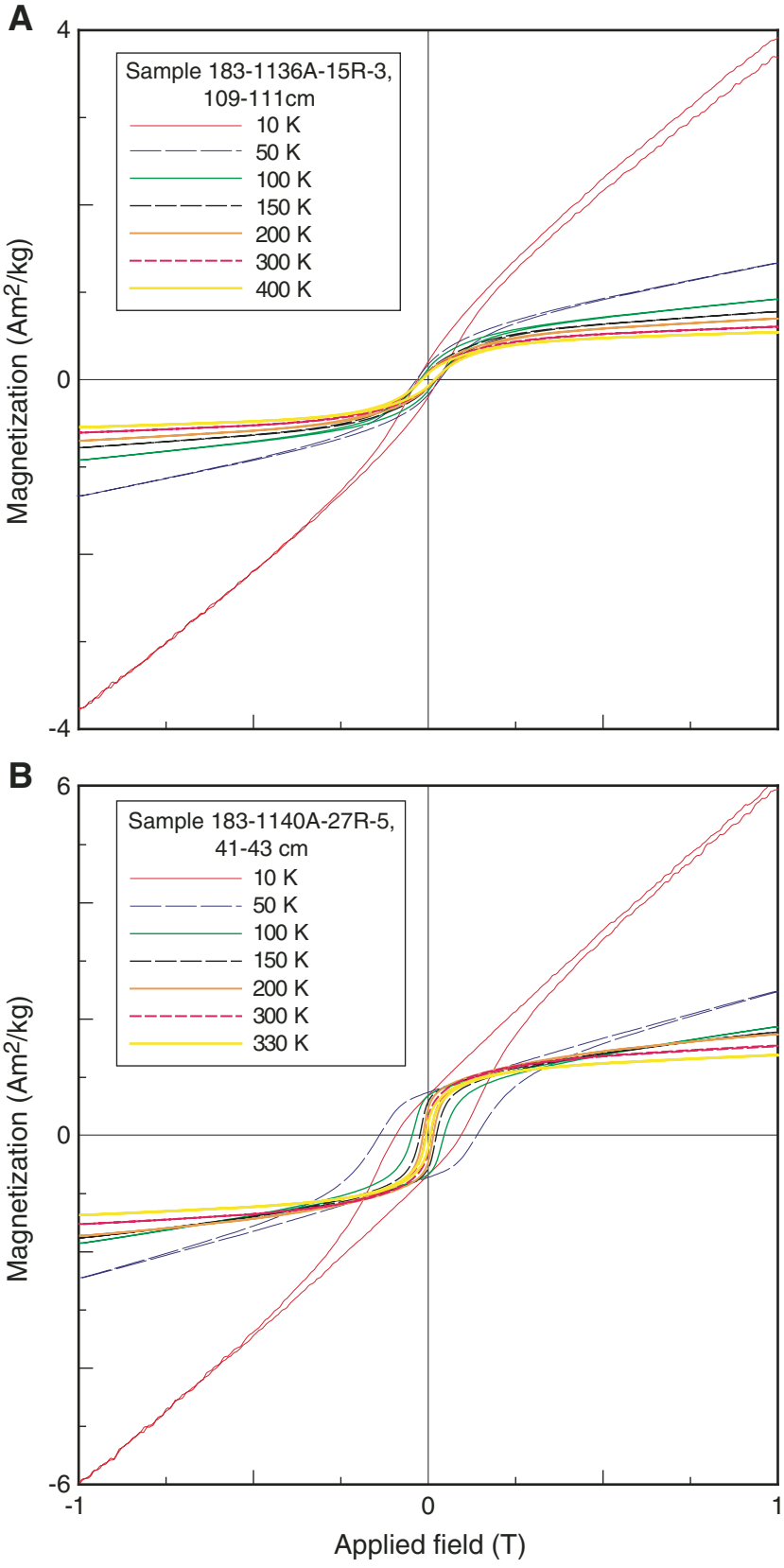

Figure F6. Low-temperature heating curves of saturation remanence for several representative samples (1 emu = 10^{-3} Am^2, SI). (**A**) Sample 183-1136A-16R-1, 134–136 cm, (**B**) Sample 183-1138A-85R-2, 89–91 cm, and (**C**) Sample 183-1140A-27R-5, 41–43 cm.

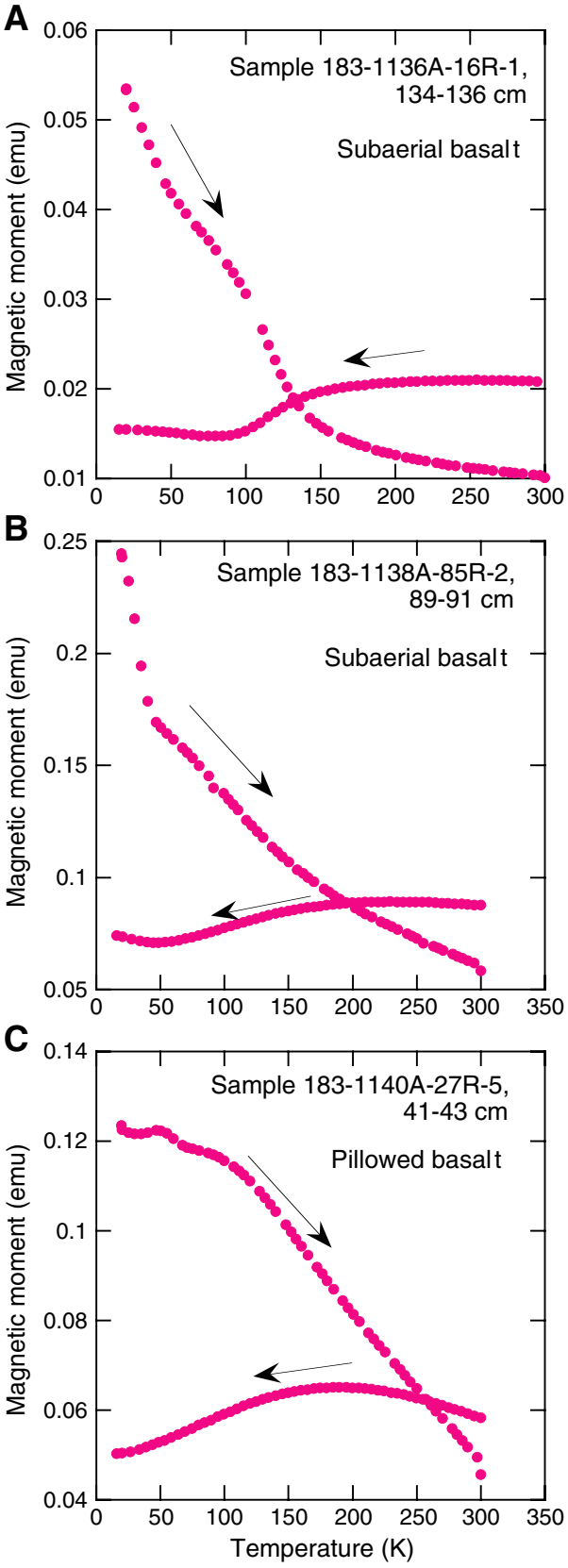

Figure F7. Diagram showing the temperature dependence of mass susceptibility for Sample 183-1141A-24R-2, 6–8 cm, during warming from 15 to 225 K. The temperature dependence of the (**A**) in-phase (m') and (**B**) quadrature (m'') mass susceptibility between 15 and 225 K was measured at five frequencies (40, 140, 400, 1000, and 4000 Hz), with AC field amplitudes between 100 and 1000 A/m.

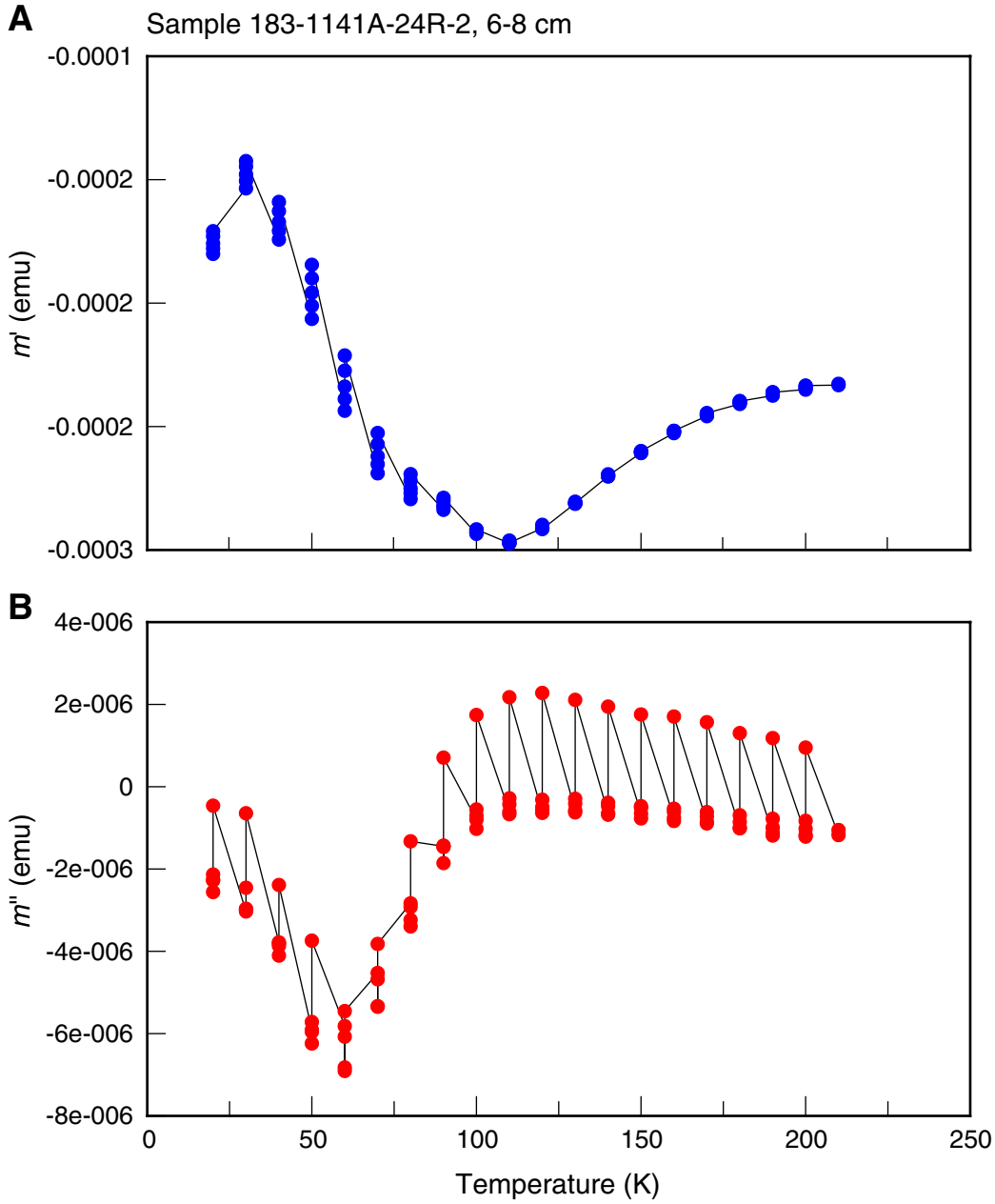

Figure F8. Diagram showing the temperature dependence of mass susceptibility for Sample 183-1140A-37R-4, 16–18 cm, during warming from 15 to 300 K. The temperature dependence of the (**A**) in-phase (*m*') and (**B**) quadrature (*m*") mass susceptibility between 15 and 300 K was measured at five frequencies (40, 140, 400, 1000, and 4000 Hz) with AC field amplitudes between 100 and 1000 A/m.

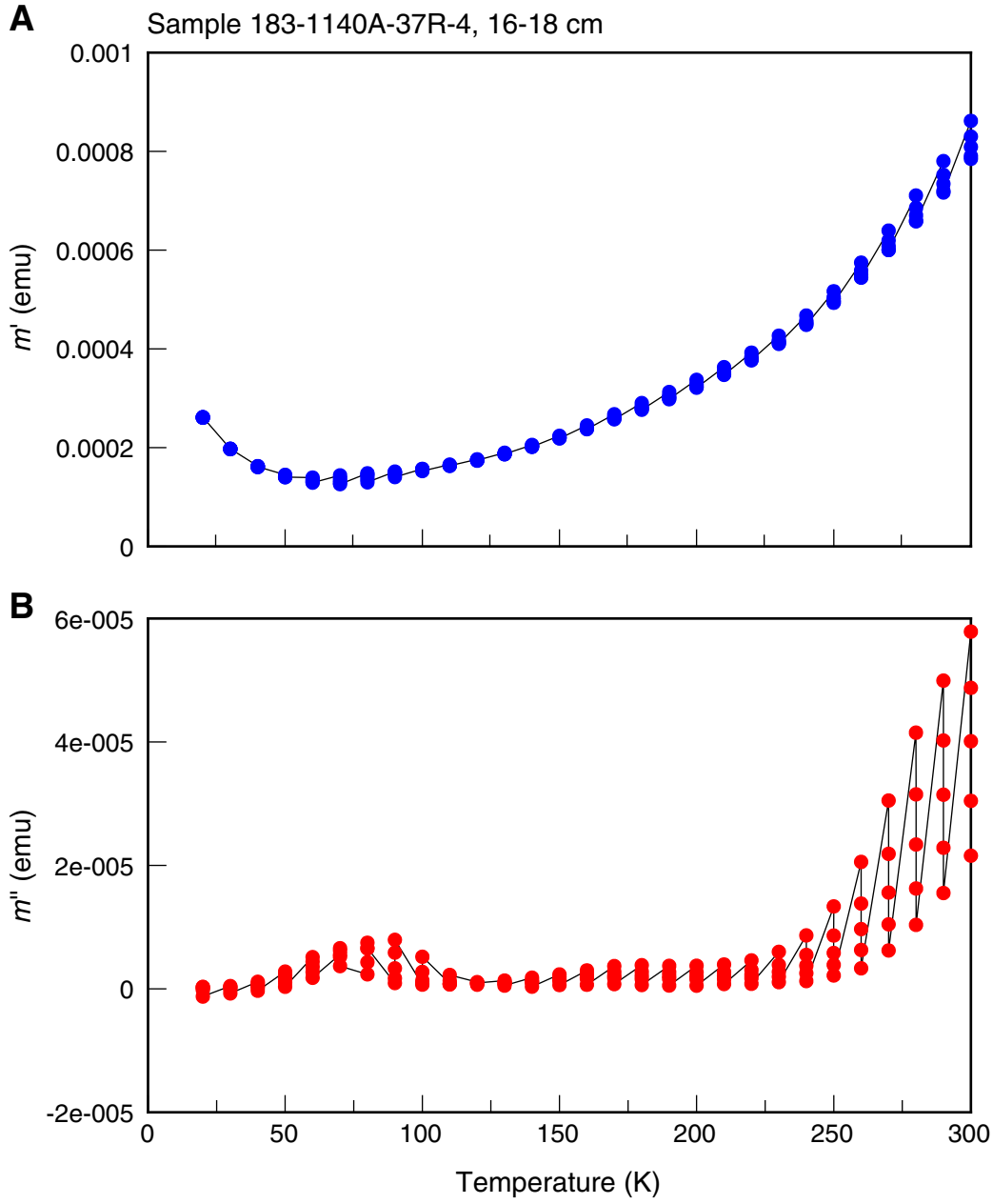

Figure F9. Mössbauer spectra of (**A**) Sample 183-1136A-16R-2, 140–142 cm (basalt sample from the Southern Kerguelen Plateau), and (**B**) Sample 183-1141A-24R-2, 6–8 cm (subaerial basalt sample from Broken Ridge).

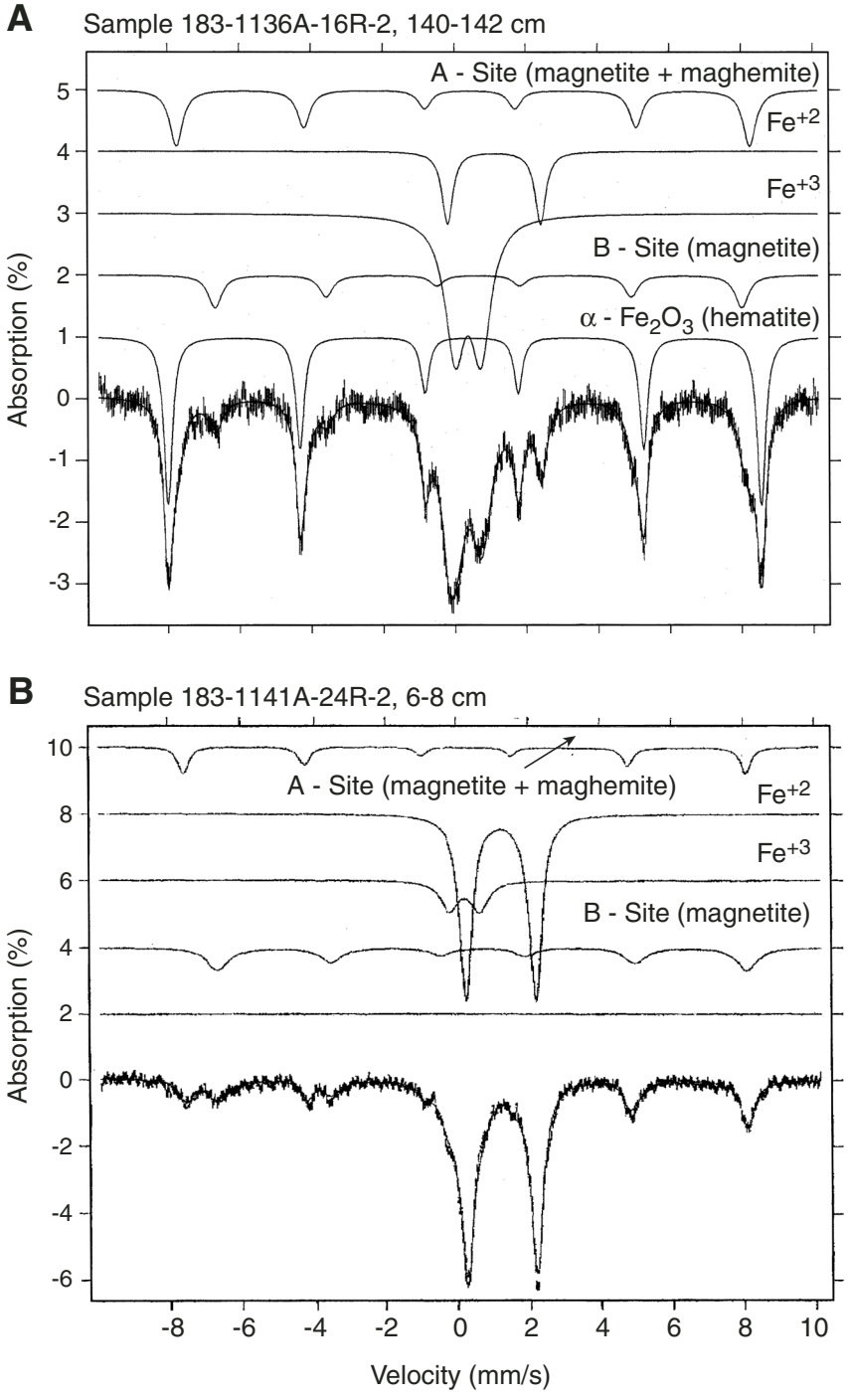

Table T1. Simplified summary of Leg 183 drill sites where volcanic rock was recovered.

Site	Location	Coordinates	Water depth (m)	Basement recovery (m)	Lithologic description	Paleoenvironment	Age (Ma)*
1136	Southern Kerguelen Plateau	59°39.1′S, 4°50.1′E	1930.6	18.4	Inflated pahoehoe flows of massive basalt	Subaerial	119
1137	Elan Bank	56°50.0′S, 68°05.6′E	1004.5	105.5	Crystal vitric tuff and brecciated basalts	Subaerial	108
1138	Central Kerguelen Plateau	53°33.1′S, 75°58.5′E	1141.4	69.0	Volcaniclastic deposits and multiple basalt flows	Subaerial	100
1139	Skiff Bank	50°11.1′S, 63°56.2′E	1415.3	87.3	Altered volcaniclastic rocks and multiple basalt flows	Subaerial	69
1140	Northern Kerguelen Plateau	46°15.6′S, 68°29.5′E	2394.1	49.1	Submarine pillow and massive basalts	Submarine	34
1141	Broken Ridge	32°13.6′S, 97°07.7′E	1196.9	39.1	Altered basalts and mafic lava flows	Subaerial	95
1142	Broken Ridge	32°13.9′S, 97°07.5′E	1200.8	17.3	Massive and pillowed basalt and volcanic breccia	Submarine?	95

Note: * = new basement ages reported by Pringle and Duncan (2000) and Figure F1, p. 15.

Table T2. Summary of Curie temperature determination of minicore samples from the Leg 183 sites. (**See table notes.** Continued on next page.)

Core, section, interval (cm)	Depth (mbsf)	Temperature* (°C)	Temperature† (°C)	Rock type	Alteration
183-1136A-					
15R-2, 44–46	128.64	—	569	Massive basalt	High
15R-2, 77–79	128.97	—	562	Massive basalt	High
15R-2, 132–134	129.52	—	572	Massive basalt	Moderate
15R-3, 109–111	130.68	—	575	Massive basalt	Slight
15R-3, 118–120	130.77	—	569	Massive basalt	Slight
15R-4, 3–5	131.09	—	554	Massive basalt	Slight
16R-1, 62–64	138.22	—	572	Massive basalt	Slight
16R-1, 134–136	138.94	560	575	Massive basalt	Slight
16R-2, 9–11	139.15	—	566	Massive basalt	Slight
16R-2, 32–34	139.38	—	567	Massive basalt	Slight
16R-2, 115–117	140.21	—	567	Massive basalt	Moderate
16R-2, 140–142	140.46	550	—	Massive basalt	Moderate
16R-3, 66–68	141.22	—	580	Massive basalt	Slight–moderate
17R-1, 20–22	144.10	—	539	Massive basalt	Slight–moderate
17R-2, 12–14	145.50	—	561	Massive basalt	Slight–moderate
17R-2, 63–65	146.01	—	534	Massive basalt	Slight–moderate
18R-1, 61–63	147.91	580	—	Massive basalt	Slight–moderate
18R-1, 75–77	148.05	—	546	Massive basalt	Slight–moderate
18R-2, 123–125	149.91	—	302	Massive basalt	Slight–moderate
18R-4, 126–128	152.05	—	265	Massive basalt with numerous veins	Slight–moderate
18R-5, 32–34	152.55	—	220	Massive basalt with numerous veins	Slight–moderate
18R-5, 130–132	153.53	—	208	Massive basalt with numerous veins	Slight–moderate
18R-6, 13–15	153.86	—	207	Massive basalt with numerous veins	Slight–moderate
19R-1, 77–79	157.67	—	244	Massive basalt with numerous veins	Slight
19R-1, 122–124	158.12	520	—	Massive basalt with numerous veins	Slight
19R-2, 45–47	158.89	—	186	Massive basalt with numerous veins	Slight
183-1137A–					
25R-3, 89–91	232.11	—	582	Basaltic breccia	Slight–moderate
27R-3, 87–89	251.45	545	—	Massive basalt	Moderate
32R-1, 58–60	276.68	505	—	Massive basalt	Slight
43R-1, 27–29	352.47	—	500?	Crystal-vitric tuff	High
43R-2, 43–45	353.48	435	620	Crystal-vitric tuff	High
45R-3, 17–19	364.44	520	575	Massive basalt	Slight
183-1138A-					
78R-1, 44–46	727.44	—	538	Pumice lithic breccia	High
79R-4, 115–117	742.02	—	334	Massive basalt	High
80R-2, 114–116	748.91	—	335	Massive basalt	Slight
81R-1, 92–94	756.82	—	563	Massive basalt	High
81R-5, 9–11	761.45	480	498	Massive basalt	Moderate
81R-5, 61–63	761.97	—	562	Massive basalt	Moderate
81R-5, 82–84	762.18	—	605	Massive basalt	Moderate
82R-3, 128–130	769.85	—	493	Massive basalt	Moderate
83R-2, 68–70	777.38	—	562	Massive basalt	Moderate
83R-5, 73–75	781.66	—	575	Massive basalt	Moderate–high
84R-1, 106–108	785.86	—	550	Massive basalt	Moderate
84R-3, 91–93	788.41	—	538	Basaltic breccia	High
85R-2, 84–86	796.67	—	501	Massive basalt	Moderate
85R-2, 89–91	796.72	—	540	Massive basalt	Slight
86R-1, 55–57	804.64	—	552	Massive basalt	Moderate–high
86R-3, 25–27	807.35	—	321	Massive basalt	Moderate
87R-2, 90–92	816.06	—	310	Massive basalt	Slight–moderate
88R-1, 53–55	823.93	—	508	Basaltic breccia	High
89R-1, 40–42	833.50	—	354	Basaltic breccia	High
89R-2, 111–113	835.69	—	332	Massive basalt	Moderate
89R-3, 40–42	836.26	480	535	Massive basalt	Moderate–high
183-1139A-					
64R-5, 0–2	610.14	510	—	Massive basalt with carbonate-filled veins	Slight–moderate
66R-3, 64–66	627.12	—	540	Massive basalt	Moderate
68R-7, 146–148	651.69	—	529	Massive tracyandesite	Moderate
71R-4, 8–10	674.28	—	547	Massive tracyandesite	Moderate–high
72R-2, 11–13	681.84	—	605	Massive trachyte	Moderate
73R-3, 37–39	692.87	560	—	Basalt with clay-filled veins	Moderate–high
183-1140A-					
25R-6, 65–67	235.18	—	245	Pillowed basalt	Slight
26R-2, 15–17	238.64	595	535	Pillowed basalt	Fresh–slight

Table T2 (continued).

Core, section, interval (cm)	Depth (mbsf)	Temperature* (°C)	Temperature† (°C)	Rock type	Alteration
27R-1, 104–106	240.34	—	157	Pillowed basalt	Slight
27R-2, 51–53	241.22	—	165	Massive basalt	Slight
27R-3, 37–39	242.36	—	571	Massive basalt	Very slight
27R-4, 4–6	243.46	—	208	Massive basalt	Fresh–slight
27R-5, 41–43	245.22	—	270	Pillowed basalt	Fresh–slight
28R-1, 58–60	247.48	—	521	Pillowed basalt	Slight
32R-1, 78–80	275.98	—	321	Massive basalt	Slight
33R-2, 61–63	286.63	—	359	Massive basalt	Slight–moderate
34R-2, 38–40	295.98	—	187	Massive basalt	Slight–moderate
34R-5, 10–12	299.51	—	289	Pillowed basalt	Slight–moderate
35R-1, 105–107	304.55	—	560	Pillowed basalt	Slight–moderate
35R-2, 24–26	305.21	—	310	Pillowed basalt	Slight–moderate
36R-3, 73–75	316.14	—	154	Massive basalt	Fresh
36R-4, 6–8	316.97	—	203	Massive basalt	Fresh–slight
37R-1, 87–89	318.17	—	329	Massive basalt	Slight
37R-4, 16–18	320.64	230	540	Pillow basalt	Slight–moderate
183-1141A-					
19R-2, 84–86	159.12	—	520	Massive basalt	Moderate–high
21R-2, 6–8	167.77	—	582	Massive basalt	Moderate
2R-3, 35–37	174.43	520	580	Massive basalt	Moderate
23R-3, 34–36	179.18	540	—	Massive basalt	High
24R-2, 6–8	182.30	—	562	Massive basalt	Moderate–high
24R-3, 85–87	184.54	525	—	Massive basalt	Moderate–high
183-1142A-					
1W-1, 35–37	90.35	—	455	Massive basalt	Slight
2R-1, 14–16	91.14	—	485	Massive basalt	Slight
2R-1, 66–68	91.66	—	463	Massive basalt	Slight
2R-1, 93–95	91.93	—	538	Massive basalt	Slight
2R-1, 102–104	92.02	—	500	Massive basalt	Slight
2R-1, 132–134	92.32	—	577	Massive basalt	Slight
3R-1, 39–41	99.09	—	575	Basalt	Moderate
5R-1, 144–146	114.54	580	—	Massive basalt	Complete
5R-2, 18–20	114.77	—	574	Massive basalt	Complete
5R-2, 58–60	115.17	—	565	Basaltic breccia	Complete
9R-1, 62–64	132.92	—	554	Pillowed basalt?	High–complete
9R-2, 126–128	135.06	—	517	Massive basalt	Moderate–very high
9R-3, 33–35	135.56	—	530	Pillowed basalt?	Moderate–very high
9R-4, 16–18	136.89	—	528	Pillowed basalt?	High
9R-4, 26–28	136.99	—	548	Pillowed basalt?	High
10R-1, 38–40	137.48	495	—	Pillowed basalt?	Moderate–high
10R-1, 65–67	137.75	—	555	Pillowed basalt?	Moderate–high
10R-1, 80–82	137.90	—	554	Pillowed basalt?	Moderate–high
10R-1, 136–138	138.46	—	555	Pillowed basalt?	Moderate–high
10R-1, 143–145	138.53	—	569	Pillowed basalt?	Moderate–high
10R-2, 54–56	139.11	—	574	Massive basalt?	Moderate–high
10R-3, 43–45	140.48	—	447	Massive basalt	Moderate

Notes: The rock type and degrees of alteration are from Coffin, Frey, Wallace, et al. (2000). * = Kappabridge. † = microvibrating Sample Magnetometer (VSM).

Table T3. Summary of hysteresis properties of minicore samples from the Leg 183 sites. (Continued on next page.)

Core, section, interval (cm)	Depth (mbsf)	H_c (mT)	H_{cr} (mT)	H_{cr}/H_c	J_r (mAm^2/kg)	J_s (mAm^2/kg)	J_r/J_s
183-1136A-							
15R-2, 44–46	128.64	33.26	59.42	1.72	97.81	341.04	0.28
15R-2, 77–79	128.97	31.78	54.81	1.68	176.67	634.41	0.30
15R-2, 132–134	129.52	33.38	56.02	1.79	164.96	550.86	0.29
15R-3, 109–111	130.68	21.03	58.13	2.76	64.43	340.82	0.19
15R-3, 111–113	130.88	20.00	52.30	2.62	78.20	450.00	0.17
15R-3, 118–120	130.77	18.84	52.72	2.80	80.52	471.63	0.17
15R-4, 3–5	131.09	20.75	42.73	2.06	67.85	259.38	0.26
16R-1, 62–64	138.22	20.83	58.88	2.83	72.80	369.94	0.20
16R-1, 80–82	138.40	21.60	55.30	2.56	66.90	350.00	0.19
16R-1, 134–136	138.94	22.91	60.61	2.65	67.92	427.48	0.16
16R-1, 136–138	139.14	23.20	55.80	2.41	70.20	406.12	0.17
16R-2, 9–11	139.15	24.59	61.41	2.50	64.43	354.36	0.18
16R-2, 32–34	139.38	24.81	59.31	2.40	67.19	355.81	0.19
16R-2, 115–117	140.21	27.94	59.50	2.13	87.18	370.38	0.24
16R-3, 66–68	141.22	14.50	28.65	1.98	138.44	774.10	0.18
16R-3, 69–71	141.25	12.70	25.4	2.00	224.00	1270.00	0.18
17R-1, 20–22	144.10	11.02	21.92	1.99	111.04	565.13	0.20
17R-2, 12–14	145.50	6.88	15.88	2.31	81.39	675.29	0.12
17R-2, 63–65	146.01	25.65	44.26	1.73	225.06	772.58	0.29
18R-1, 75–77	148.05	17.61	46.48	2.64	135.81	803.99	0.17
18R-2, 123–125	149.91	9.47	14.67	1.55	96.28	386.30	0.25
18R-4, 126–128	152.05	12.33	17.72	1.44	48.71	140.37	0.35
18R-5, 32–34	152.55	9.10	12.89	1.42	60.86	230.46	0.27
18R-5, 130–132	153.53	16.27	22.36	1.37	94.46	233.38	0.41
18R-6, 13–15	153.86	15.37	28.98	1.89	97.26	260.12	0.37
19R-1, 77–79	157.67	7.58	11.05	1.46	51.49	227.55	0.23
19R-2, 45–47	158.89	5.94	9.14	1.54	52.72	274.66	0.19
183-1137A-							
25R-3, 89–91	232.11	11.9	26.4	2.22	129.00	928.00	0.14
43R-1, 27–29	352.47	15.4	30.3	1.97	0.80	4.36	0.18
43R-2, 43–45	353.48	9.48	32.5	3.43	10.40	102.00	0.10
45R-3, 17–19	364.44	10.10	23.40	2.32	168.00	1200.00	0.14
183-1138A-							
78R-1, 44–46	727.44	17.63	39.32	2.23	48.31	238.59	0.20
79R-4, 115–117	742.02	6.41	14.46	2.26	73.68	239.05	0.14
80R-2, 114–116	748.91	10.18	22.23	2.18	174.47	1003.17	0.17
80R-4, 65–67	751.35	7.62	17.00	2.23	114.92	840.39	0.14
81R-1, 92–94	756.82	16.02	30.84	1.93	228.24	923.26	0.25
81R-4, 27–29	760.38	27.60	41.20	1.49	1010.00	3330.00	0.30
81R-5, 9–11	761.45	7.87	20.97	2.67	233.63	2194.68	0.11
81R-5, 61–63	761.97	7.94	17.00	2.14	289.00	1880.00	0.15
82R-1, 42–44	766.02	8.63	39.72	4.60	99.70	1046.80	0.10
82R-3, 128–130	769.85	4.53	14.70	3.24	169.01	2486.24	0.07
83R-2, 68–70	777.38	8.28	19.59	2.36	204.47	1185.76	0.17
83R-5, 73–75	781.66	17.01	33.77	1.99	523.61	2385.75	0.22
84R-1, 106–108	785.86	9.17	19.72	2.15	195.08	1208.93	0.16
84R-3, 91–93	788.41	11.35	37.78	3.33	77.40	531.06	0.15
85R-2, 84–86	796.67	7.08	18.76	2.65	272.57	2123.22	0.13
85R-2, 89–91	796.72	4.89	11.60	2.37	281.00	2420.00	0.12
86R-1, 55–57	804.64	10.85	23.76	2.19	394.78	1587.84	0.25
86R-3, 25–27	807.35	4.48	9.94	2.22	168.34	1555.92	0.11
87R-2, 90–92	816.06	5.99	10.67	1.78	205.80	1262.30	0.16
88R-1, 53–55	823.93	7.34	17.32	2.36	262.56	1996.38	0.13
89R-1, 40–42	833.50	7.72	18.88	2.45	153.80	1041.09	0.15
89R-2, 111–113	835.69	8.59	20.53	2.19	197.67	1081.53	0.18
89R-3, 40–42	836.26	6.56	12.30	1.88	192.00	1160.00	0.17
183-1139A-							
66R-3, 64–66	627.12	4.15	12.00	2.89	171.00	2050.00	0.08
68R-7, 146–148	651.69	4.44	19.00	4.28	205.07	3722.00	0.06
71R-4, 8–10	674.28	34.00	111.00	3.26	9.00	30.50	0.30
71R-7, 29–31	678.74	118.00	322.00	2.73	2.12	4.41	0.48
72R-2, 11–13	681.84	14.70	64.70	4.40	10.60	75.50	0.14
73R-3, 37–39	692.87	176.00	232.00	1.32	3.00	3.69	0.81
183-1140A-							
25R-6, 65–67	235.18	13.83	20.05	1.45	207.22	539.98	0.38

Table T3 (continued).

Core, section, interval (cm)	Depth (mbsf)	H_c (mT)	H_{cr} (mT)	H_{cr}/H_c	J_r (mAm^2/kg)	J_s (mAm^2/kg)	J_r/J_s
26R-2, 15–17	238.64	20.110	23.10	1.15	211.00	431.00	0.49
27R-1, 104–106	240.34	7.16	11.18	1.56	132.04	573.86	0.23
27R-2, 51–53	241.22	5.80	10.95	1.89	95.52	643.61	0.15
27R-3, 37–39	242.36	4.69	9.71	2.07	100.03	784.66	0.13
27R-4, 4–6	243.46	5.62	10.54	1.87	113.30	741.96	0.15
27R-5, 41–43	245.22	7.34	11.90	1.62	227.00	1020.00	0.22
28R-1, 58–60	247.48	19.64	22.21	1.13	143.96	242.67	0.59
31R-1, 69–71	275.89	34.87	44.95	1.29	118.94	212.44	0.56
32R-1, 78–80	275.98	9.99	13.69	1.37	263.30	815.72	0.32
33R-2, 61–63	286.63	6.98	10.50	1.50	133.44	586.68	0.23
34R-5, 10–12	299.51	11.90	15.46	1.30	175.34	417.86	0.42
35R-1, 105–107	304.55	8.68	10.80	1.24	179.00	523.00	0.34
35R-2, 24–26	305.21	7.50	10.48	1.40	146.77	568.24	0.26
36R-3, 73–75	316.14	4.54	9.13	2.01	104.67	794.47	0.13
36R-4, 6–8	316.97	5.24	10.87	2.07	103.54	784.84	0.13
37R-1, 87–89	318.17	6.91	10.13	1.47	127.37	584.46	0.22
37R-4, 16–18	320.64	6.95	11.20	1.61	177.0	872.00	0.20
183-1141A-							
19R-2, 84–86	159.12	13.00	23.90	1.84	13.60	89.10	0.15
21R-2, 6–8	167.77	17.00	32.00	1.88	46.90	266.00	0.18
22R-3, 35–37	174.43	10.40	29.90	2.88	59.20	547.00	0.11
24R-2, 6–8	182.30	4.20	12.90	3.07	48.10	667.00	0.07
183-1142A-							
1R-1, 35–37	90.35	6.71	15.05	2.24	102.38	719.09	0.14
2R-1, 66–68	91.66	7.02	14.93	2.13	115.91	920.06	0.13
2R-1, 93–95	91.93	10.28	20.01	1.95	7.20	37.63	0.19
2R-1, 102–104	92.02	10.24	19.88	1.94	85.83	450.11	0.19
2R-1, 132–134	92.32	12.61	29.66	2.35	20.16	85.99	0.23
3R-1, 39–41	99.09	3.78	22.20	5.87	156.00	4560.00	0.03
5R-1, 144–146	114.54	35.65	77.91	2.19	55.33	127.58	0.43
5R-2, 18–20	114.77	16.99	51.29	3.02	81.05	452.02	0.18
5R-2, 58–60	115.17	25.58	—	—	40.46	159.49	0.25
9R-1, 62–64	132.92	3.83	19.64	5.13	216.88	6154.74	0.04
9R-2, 126–128	135.06	3.58	15.95	4.45	130.38	3161.09	0.04
9R-3, 33–35	135.56	3.51	12.80	3.65	150.00	2850.00	0.05
9R-4, 16–18	136.89	4.89	19.22	3.93	171.05	2953.06	0.06
9R-4, 26–28	136.99	5.74	21.47	3.74	207.79	3340.46	0.06
10R-1, 65–67	137.75	4.57	18.62	4.07	134.59	2269.63	0.06
10R-1, 80–82	137.90	5.16	18.08	3.51	243.17	3752.54	0.06
10R-1, 136–138	138.46	13.11	39.96	3.05	207.64	1495.43	0.14
10R-1, 143–145	138.53	5.89	22.34	3.79	250.62	4450.05	0.06
10R-2, 54–56	139.11	5.73	20.27	3.54	244.59	3919.92	0.06
10R-3, 43–45	140.48	3.95	16.48	4.17	123.22	2097.25	0.06